

Projected Constraints on Modified Gravity Cosmologies from 21 cm Intensity Mapping

Kiyoshi Wesley Masui,^{1,2,*} Fabian Schmidt,^{3,†} Ue-Li Pen,^{1,‡} and Patrick McDonald^{1,§}

¹*Canadian Institute for Theoretical Astrophysics,*

60 St. George Street Toronto, Ontario, M5S 3H8, Canada

²*Department of Physics, University of Toronto, 60 St. George Street Toronto, Ontario, M5S 1A7, Canada*

³*Theoretical Astrophysics, California Institute of Technology M/C 35 0-17, Pasadena, California 91125-0001, USA*

(Dated: February 9, 2010)

We present projected constraints on modified gravity models from the observational technique known as 21 cm intensity mapping, where cosmic structure is detected without resolving individual galaxies. The resulting map is sensitive to both BAO and weak lensing, two of the most powerful cosmological probes. It is found that a 200 m \times 200 m cylindrical telescope, sensitive out to $z = 2.5$, would be able to distinguish DGP from most dark energy models, and constrain the Hu & Sawicki $f(R)$ model to $|f_{R0}| < 9 \times 10^{-6}$ at 95% confidence. The latter constraint makes extensive use of the lensing spectrum in the nonlinear regime. These results show that 21 cm intensity mapping is not only sensitive to modifications of the standard model's expansion history, but also to structure growth. This makes intensity mapping a powerful and economical technique, achievable on much shorter time scales than optical experiments that would probe the same era.

I. INTRODUCTION

One of the greatest open questions in cosmology is the cause of the observed late time acceleration of the universe. Within the context of normal gravity described by Einstein's General Relativity, this phenomena can only be explained by an exotic form of matter with negative pressure. Another possible explanation is that on cosmological scales, General Relativity fails and must be replaced by some theory of modified gravity.

Several approaches have been proposed to modify gravity at late times to explain the apparent acceleration of the universe. The challenge in these modifications is to preserve successful predictions of the CMB at $z \approx 1000$, and also the precision tests at the present epoch in the solar system.

A generic class of theories operates with the Chameleon effect, where at sufficiently high densities General Relativity (GR) is restored, thus applying both in the solar system and the early universe. To further understand the nature of gravity would require probing gravity on cosmological scales. Large scales means large volume, requiring large fractions of the sky. Gravity can be probed by gravitational lensing, which measures geodesics and thus the gravitational curvature of space, and is a sensitive probe of the growth of structure in the Universe [1–4].

In working out predictions for cosmology, the theoretical challenge posed by these theories are the nonlinear mechanisms in each model, necessary in order to restore Einstein Gravity locally to satisfy Solar System

constraints. We present quantitative results from nonlinear calculations for a specific $f(R)$ model, and forecasted constraints for future 21 cm experiments.

An upcoming class of experiments propose the observation of the 21 cm spectral line at low resolution over a large fraction of the sky and large range of redshifts [5]. Large scale structure is detected in three dimensions without the detection of individual galaxies. This process is referred to as *21 cm intensity mapping*. These experiments are sensitive to structures at a redshift range that is observationally difficult to observe for ground-based optical experiments due to a lack of spectral lines. Yet these experiments are extremely economical [6] since they only require limited resolution and no moving parts.

Intensity mapping is sensitive to both the Baryon Acoustic Oscillations (BAO) and to weak lensing, two of the most powerful observational methods to determine cosmological parameters. It has been shown that BAO detections from 21 cm intensity mapping are powerful probes of dark energy, comparing favourably with Dark Energy Task Force Stage IV projects within the figure of merit framework [7, 8].

In this paper we present projected constraints on modified gravity models from 21 cm intensity mapping. In Section II we describe the modified gravity models considered. In Section III we discuss the observational signatures accessible to 21 cm intensity mapping, and calculate the effects of modified gravity on these signatures. In Section IV we present statistical analysis and results and we conclude in Section V.

We assume a fiducial Λ CDM cosmology with WMAP5 cosmological parameters: $\Omega_m = 0.258$, $\Omega_b = 0.0441$, $\Omega_\Lambda = 0.742$, $h = 0.719$, $n_s = 0.963$ and $\log_{10} A_s = -8.65$. We will follow the convention that $\omega_x \equiv h^2 \Omega_x$.

*Electronic address: kiyoi@cita.utoronto.ca

†Electronic address: fabians@caltech.edu

‡Electronic address: pen@cita.utoronto.ca

§Electronic address: pmcdonal@cita.utoronto.ca

II. MODIFIED GRAVITY MODELS

Here we describe some popular modified gravity models for which projected constraints will later be derived. Throughout we will use units in which $G = c = \hbar = 1$ and will be using a metric with mostly negative signature: $(+, -, -, -)$.

A. $f(R)$ Models

In the $f(R)$ paradigm, modifications to gravity are introduced by changing the standard Einstein-Hilbert action, which is linear in R , the Ricci scalar. The modifications are made by adding an additional non linear function of R [9–11]

$$S = \int d^4x \sqrt{-g} \left[\frac{R + f(R)}{16\pi} + \mathcal{L}_m \right] \quad (1)$$

where \mathcal{L}_m is the matter Lagrangian. See [12] for a comprehensive review of $f(R)$ theories of gravity.

The choice of the function $f(R)$ is arbitrary, but in practice it is highly constrained by precise solar system and cosmological constraints, as well as stability criteria [13, 14] (see below). In this paper, we choose parameterizations of $f(R)$ such that it asymptotes to a constant for a certain choice of parameters and thus approaches the fiducial Λ CDM.

In general, $f(R)$ models have enough freedom to mimic exactly the Λ CDM expansion history and yet still impose a significant modification to gravity [15, 16]. As such probes of the expansion history are less constraining than probes of structure growth, which will be evident in the constraints presented in later sections.

Variation of the above action yields the modified Einstein Equations

$$G_{\mu\nu} + f_R R_{\mu\nu} - \left(\frac{f}{2} - \square f_R \right) g_{\mu\nu} - \nabla_\mu \nabla_\nu f_R = 8\pi T_{\mu\nu} \quad (2)$$

where $f_R \equiv df(R)/dR$, a convention that will be used throughout. $f(R)$ gravity is equivalent to a scalar-tensor theory [13, 17] with the scalar field f_R having a mass and potential determined by the functional form of $f(R)$. The field has a Compton wavelength given by its inverse mass

$$\lambda_C = \frac{1}{m_{f_R}} = \sqrt{3f_{RR}}. \quad (3)$$

The main criterion for stability of the $f(R)$ model is that the mass squared of the f_R field is positive, i.e. $f_{RR} > 0$. In most cases, this simply corresponds to a sign choice for the field f_R (specifically for the model we consider below, f_{R0} is constrained to be less than 0).

On scales smaller than λ_C , gravitational forces are enhanced by 4/3, while they reduce to unmodified gravity on larger scales. The reach of the modified forces λ_C

generically leads to a scale-dependent growth in $f(R)$ models.

While the dynamics are significantly changed in $f(R)$, the relation between matter and the lensing potential is unchanged up to a rescaling of the gravitational constant by the linear contribution in f . The fractional change is of order the background field value $\bar{f}_R \equiv f_R(\bar{R}) \ll 1$ where \bar{R} is the background curvature scalar.

Proceeding further requires a choice of the functional form for f . A functional form is considered which is representative of many other cases.

Hu and Sawicki proposed a simple functional form for $f(R)$ [18], which can be written as

$$f(R) = -R_0 \frac{c_1(R/R_0)^n}{c_2(R/R_0)^n + 1}, \quad (4)$$

where we have used the value of the scalar curvature in the background today, $R_0 \equiv \bar{R}|_{z=0}$ for convenience. This three parameter model passes all stability criteria for positive n , c_1 and c_2 . One parameter can be fixed by demanding the expansion history to be close (within observational limits) to Λ CDM. In this case, Equation 4 can be conveniently reparametrized and approximated by

$$f(R) \approx -2\Lambda - \frac{f_{R0}R_0}{n} \left(\frac{R_0}{R} \right)^n. \quad (5)$$

Here Λ and f_{R0} —the value of the f_R field in the background today—have been used to parameterize the function in lieu of c_1 and c_2 . This approximation is valid as long as $|f_{R0}| \ll 1$, which is necessary to satisfy current observational constraints [18, 19]. While Λ is conceptually different than vacuum energy, it is mathematically identical and will thus be absorbed into the right hand side of the Friedmann equation and parameterized by Ω_Λ . In quoting constraints, we will marginalize over this parameter as it is of no use in identifying signatures of modified gravity. The parameter f_{R0} can be thought of as controlling the strength of modifications to gravity today, while higher n pushes these modifications to later times. The effects of changing these parameters are discussed in greater detail in [18].

Allowed $f(R)$ models exhibit the so-called chameleon mechanism: the f_R field becomes very massive in dense environments and effectively decouples from matter. This effect is active whenever the Newtonian potential is of order the background f_R field. Since cosmological potential wells are typically of order 10^{-5} for massive halos, the chameleon effect becomes important if $|\bar{f}_R| \lesssim 10^{-5}$. If the background field is $\sim 10^{-7}$ or smaller, a large fraction of the collapsed structures in the universe are chameleon-screened, so that the model becomes observationally indistinguishable from Λ CDM.

Since the chameleon effect will affect the formation of structure, standard fitting formulas based on ordinary GR simulations, such as those mapping the linear to the

nonlinear power spectrum, cannot be used for these models. Recently, however, self-consistent N-body simulations of $f(R)$ gravity have been performed which include the chameleon mechanism [20–22]. We will use the simulation results for forecasts of weak lensing in the nonlinear regime below.

It should be noted that $f(R)$ models are not without difficulties. In particular, an open issue is the problem of potential unprotected singularities [23–25].

B. DGP Braneworld

A theory of gravity proposed by Dvali, Gabadadze and Porrati (DGP) assumes that our four dimensional universe sits on a brane in five dimensional Minkowski space [26]. On small scales gravity is four dimensional but, on larger scales it becomes fully five dimensional. Here we parameterize DGP by r_c , the scale at which gravity crosses over in dimensionality. The DGP model has two branches depending on the embedding of the brane in 5D space. In the self-accelerating branch, the universe accelerates without need for a cosmological constant if $r_c \sim 1/H_0$ [27, 28]. In this branch, assuming a spatially flat Universe for now, the modified Friedmann equation is given by

$$H^2 - \frac{H}{r_c} = \frac{8\pi}{3}\bar{\rho}, \quad (6)$$

which clearly differs from Λ CDM. Thus, in contrast to the other models considered here, DGP without a cosmological constant does not reduce to Λ CDM and it is possible to completely rule out this scenario (where the others can only be constrained). In fact DGP (without a cosmological constant) has been shown to be in conflict with current data [29]. It is presented here largely for illustrative purposes.

On scales much smaller than r_c , gravity is four-dimensional but not GR. On these scales, DGP can be described as an effective scalar-tensor theory [30–32]. The massless scalar field, the brane-bending mode, is repulsive in the self-accelerating branch of DGP. Hence, structure formation is slowed in DGP when compared to an effective smooth Dark Energy model with the same expansion history. While the growth of structure is thus modified in DGP even on scales much smaller than r_c , gravitational lensing is unchanged. In other words, the relation between matter overdensities and the lensing potential is the same as in GR [33].

As in $f(R)$, the DGP model contains a nonlinear mechanism to restore GR locally. This Vainshtein mechanism is due to self-interactions of the scalar brane-bending mode which generally become important as soon as the density field becomes of order unity. In the Vainshtein regime, second derivatives of the field saturate, and thus modified gravity effects are highly suppressed in high-density regions [31, 33, 34]. We will only consider linear predictions for the DGP model here.

III. OBSERVATIONAL SIGNATURES

In this Section we describe the observational signatures available to 21 cm intensity mapping. We also give details on calculating the observables within modified gravity models. We consider two types of measurements: the Baryon Acoustic Oscillations and weak gravitational lensing.

For the fiducial survey, we assume a $200 \text{ m} \times 200 \text{ m}$ cylindrical telescope, as in [7]. We will also present limited results for a $100 \text{ m} \times 100 \text{ m}$ cylindrical telescope to illustrate effects of reduced resolution and collecting area on the results. This latter case is representative of first generation projects [6]. In the 200 m case we assume 4000 receivers, and in the 100m case 1000 receivers. We assume either telescope covers 15000 sq. deg. over 4 years. We assume neutral hydrogen fraction and the bias remain constant with $\Omega_{\text{HI}} = 0.0005$ today and $b = 1$. The object number density is assumed to be $\bar{n} = 0.03$ per cubic $h^{-1}\text{Mpc}$ (effectively no shot-noise, as should be the case in practice [7]).

A. Baryonic acoustic oscillation expansion history test

Acoustic oscillations in the primordial photon-baryon plasma have ubiquitously left a distinctive imprint in the distribution of matter in the universe today. This process is understood from first principles and gives a clean length scale in the universe’s large scale structure, largely free of systematic uncertainties and calibrations. This can be used to measure the global cosmological expansion history through the angular diameter distance, d_A , and Hubble parameter, H , vs redshift relation. The detailed expansion and acceleration will differ between pure cosmological constant and modified gravity models.

We use essentially the method of [35] for estimating distance errors obtainable from a BAO measurement, including 50% reconstruction of nonlinear degradation of the BAO feature. We assume the frequency range corresponding to $z < 2.5$ is covered (the lower z end should be covered by equivalent galaxy redshift surveys if not a 21cm survey). For the sky area and redshift range surveyed, the 200m telescope is nearly equivalent to a perfect BAO measurement. The limited resolution and collecting area of the 100m telescope substantially degrades the measurement at the high- z end.

The expansion history for modified gravity models can be calculated in an analogous way to that in General Relativity. The Friedmann Equation in DGP, Equation 6 can be written as

$$H^2 = -\frac{k}{a^2} + \left(\frac{1}{2r_c} + \sqrt{\frac{1}{4r_c^2} + \frac{8\pi\bar{\rho}}{3}} \right)^2 \quad (7)$$

where k is the curvature, and r_c is the crossover scale. It is convenient to introduce the parameter $\omega_{rc} \equiv 1/4r_c^2$

which stands in for r_c . This equation can be solved numerically to calculate the observable quantities.

We now calculate the expansion history in the HS $f(R)$ model using a perturbative framework which is well suited for calculating constraints on f_{R0} . Working in the conformal gauge and mostly negative signature, we start with the modified Einstein's Equation (2). At zeroth order the left hand side of the 00 component contains the modified Friedmann equation

$$H^2 = \frac{8\pi\bar{\rho}}{3} + f_{R0}g_n(a, \dot{a}, \ddot{a}, \ddot{\ddot{a}}) \quad (8)$$

where $\bar{\rho}$ is the average density (including contributions from Λ), the over-dot represents a conformal derivative and

$$g_n \equiv \frac{-1}{f_{R0}a^2} \left[\frac{(\bar{f} + 2\Lambda)a^2}{6} + \bar{f}_R \left(\frac{\dot{a}^2}{a^2} - \frac{\ddot{a}}{a} \right) + 6\bar{f}_{RR} \left(\frac{\ddot{a}\dot{a}}{a^4} - \frac{3\ddot{a}\dot{a}^2}{a^5} \right) \right]. \quad (9)$$

For verifiability we quote

$$g_1 = \frac{a^2 R_0^2 (2a\ddot{a}^2 - 7\ddot{a}\dot{a}^2 + 2\ddot{\ddot{a}}\dot{a}a)}{36\ddot{a}^3}. \quad (10)$$

Evaluating Equation 8 at the present epoch yields the modified version of the standard constraint

$$h^2 = \omega_m + \omega_r + \omega_k + \omega_\Lambda + f_{R0}g_{n0}. \quad (11)$$

Note that the modified version of the Friedmann Equation is third order instead of first order, however, it has been shown that the expansion history stably approaches that of Λ CDM for vanishing f_{R0} [18]. For observationally allowed cosmologies $f_{R0} \ll 1$ we expand

$$f_{R0}g_n = f_{R0}g_n(\tilde{a}, \dot{\tilde{a}}, \ddot{\tilde{a}}, \ddot{\ddot{\tilde{a}}}) + O(f_{R0}^2) \quad (12)$$

where \tilde{a} is the solution to the *standard* GR Friedmann equation.

By using Equation 12 in Equation 8 and keeping only terms linear in f_{R0} , the expansion history can be calculated in the regular way, along with the observable quantities $d_A(z)$ and $H(z)$. For small f_{R0} this agrees well with the calculation in [18] where the full third order differential equation was integrated

In calculating the Fisher Matrix, this treatment is exact because the Fisher Matrix depends only on the first derivative of the observables with respect to the model parameters, evaluated at the fiducial model.

B. Weak Lensing

A second class of observables measures the spatial perturbations in the gravitational metric. Modified gravity will change the strength of gravity on large scales and thus modify the growth of cosmological structure. Weak

gravitational lensing, the gravitational bending of source light by intervening matter, is a probe of this effect.

Weak lensing measures the distortion of background structures as their light propagates to us. Here, the background structure is the 21 cm emission from unresolved sources. While light rays are deflected by gravitational forces, this deflection is not directly observable, since we don't know the primary unlensed 21 cm sky. However, weak lensing will induce correlations in the measured 21 cm background, since neighbouring rays pass through common lens planes. While the deflection angles themselves are small (of order arcseconds) the deflections are coherent over scales of arcminutes. In this way, the lensing signal can be extracted statistically using quadratic estimators [36]. Given the smallness of the lensing effect, a high resolution (high equivalent number density of "sources") is necessary to detect the effect.

The weak lensing observable that is predicted by theory is the power spectrum of the convergence κ . It is given by

$$C^{\kappa\kappa}(\ell) = \left(\frac{3}{2} \Omega_m H_0^2 \right)^2 \int_0^{\chi_s} \frac{d\chi}{\chi} \frac{W_L(\chi)^2}{\chi a^2(\chi)} \epsilon^2(\chi) P(\ell/\chi; \chi) \quad (13)$$

where χ denotes comoving distances, $P(k, \chi)$ is the (linear or nonlinear) matter power spectrum at the given redshift, and we have assumed flat space. The lensing weight function $W_L(\chi)$ is given by:

$$W_L(\chi) = \int_{z(\chi)}^\infty dz_s \frac{\chi}{\chi(z_s)} (\chi(z_s) - \chi) \frac{dN}{dz}(z_s). \quad (14)$$

Here, dN/dz is the redshift distribution of source galaxies, normalized to unity. The factor $\epsilon(\chi)$ in Equation 13 encodes possible modifications to the Poisson equation relating the lensing potential to matter (Section II). In $f(R)$, it is given by $\epsilon(\chi) = (1 + \bar{f}_R(\chi))^{-1}$, while $\epsilon = 1$ for GR as well as DGP. Note that for viable $f(R)$ models, $\epsilon - 1 \lesssim 0.01$, so the effect of ϵ on the lensing power spectra is very small.

The CAMB Sources module [37, 38] was used to calculate the lensing convergence power spectrum in flat Λ CDM models. The HALOFIT [39] interface for CAMB was used for calculations that include lensing at nonlinear scales.

For the modified gravity models in the linear regime, the convergence power spectra were calculated using the Parametrized Post-Friedmann (PPF) approach [40] as in [4]. Briefly, the PPF approach uses an interpolation between super-horizon scales and the quasi-static limit. On super-horizon scales ($k \ll aH$), specifying the background expansion history, together with a relation between the two metric potentials, already determines the evolution of metric and density perturbations. On small scales ($k \gg aH$), time derivatives in the equations for the metric perturbations can be neglected with respect to spatial derivatives, leading to a modified Poisson equation for the metric potentials. The PPF approach uses a simple interpolation scheme between these limits, with a

few fitting parameters adjusted to match the full calculations [40]. The full calculations are reproduced to within a few percent accuracy. We use the transfer function of [41] to calculate the Λ CDM power spectrum at an initial redshift of $z_i = 40$, where modified gravity effects are negligible, and evolve forward using the PPF equations.

For the $f(R)$ model, we also calculate predictions in the nonlinear regime. For these, we use simulations of the HS model with $n = 1$ and f_{R0} values ranging from 10^{-6} to 10^{-4} . We use the deviation $\Delta P(k)/P(k)$ of the nonlinear matter power spectrum measured in $f(R)$ simulations from that of Λ CDM simulations with the same initial conditions [21]. This deviation is measured more precisely than $P(k)$ itself. We then spline-interpolate the measurements of $\Delta P(k)/P(k)$ for $k = 0.04 - 3.1 h/\text{Mpc}$ and at scale factors $a = 0.1, 0.2, \dots, 1.0$, and multiply the standard nonlinear Λ CDM prediction (HALOFIT) with this value. For values of $k > 3.1 h/\text{Mpc}$, we simply set $\Delta P(k) = 0$. However, for the angular scales and redshifts considered here ($\ell < 600$, see below), such high values of k do not contribute significantly.

One might be concerned that this mixing of methods, for calculating the lensing spectrum, might artificially exaggerate the effects of modified gravity if these methods do not agree perfectly. While the spectra calculated for the fiducial Λ CDM model differed by up to a percent between these methods, presumably due to slight differences in the transfer function, this should have no effect on the results. Any direct comparison between spectra (for example finite difference derivatives) are made between spectra calculated in the same manner. Note that the Fisher Matrix depends only on the first derivative of the observables with respect to the parameters and no cross derivatives are needed.

The lensing spectra were not calculated for non-flat models, but it is expected that the CMB and BAO are much more sensitive to the curvature and as such the lensing spectra are relatively unaffected. Formally we are assuming that

$$\frac{\sigma_{\omega_k}}{\sigma_{C^{\kappa\kappa}}} \frac{\partial C^{\kappa\kappa}}{\partial \omega_k} \ll 1.$$

Reconstructing weak lensing from 21 cm intensity maps involves the use of quadratic estimators to estimate the convergence and shear fields. The accuracy with which this can be done increases with information in the source maps, however, this information saturates at small scales due to nonlinear evolution. As such, one cannot improve the lensing measurement indefinitely by increasing resolution, and the experiments considered here extract much of the available information within the redshift range considered.

The accuracy with which the convergence power spectrum can be reconstructed from 21 cm intensity maps was derived in [36], where the effective lensing galaxy density was calculated at redshifts 1.25, 3 and 5 (see Figure 7 and Table 2 therein). The effective volume galaxy density was corrected for the finite resolution of the experiment con-

sidered here. It was then interpolated, using a piecewise power law, and integrated from redshift 1 to 2.5 to obtain an effective area galaxy density of $n_g/\sigma_e^2 = 0.37 \text{ arcmin}^{-2}$. The parameter σ_e^2 is the variance in the intrinsic galaxy ellipticity, which is only used here for comparison with optical weak lensing surveys. From the effective galaxy density the error on the convergence power is given by

$$\Delta C^{\kappa\kappa}(\ell) = \sqrt{\frac{2}{(2\ell+1)f_{sky}}} \left(C^{\kappa\kappa}(\ell) + \frac{\sigma_e^2}{n_g} \right) \quad (15)$$

where f_{sky} is the fraction of the sky surveyed. The galaxy distribution function dN/dz used to calculate the theoretical curves (from Equation 13) should follow the effective galaxy density. Instead for simplicity, a flat step function was used, with this distribution function equal from redshift 1 to 2.5 and zero elsewhere. While the difference between these distributions would have an effect on the lensing spectra, the effect on differences of spectra when varying parameters is expected to be negligible. Our approximation is also conservative, since the proper distribution function is more heavily weighted toward high redshift. Rays travelling from high redshift will be affected by more intervening matter and thus experience more lensing. This would increase the lensing signal, allowing a more precise measurement.

Figure 1 shows the lensing spectra for the fiducial cosmology and a modified gravity model, including both linear and nonlinear calculations. The linear regime is taken to be up to $\ell = 140$ for projected constraints. For calculations including weak lensing in the nonlinear regime, $C^{\kappa\kappa}(\ell)$ up to $\ell = 600$ is used for the larger telescope. Beyond this scale the model used for lensing error-bars is not considered accurate at the shallowest redshifts in the source window [36]. This cut off coincides with the scale at which information in the source structures saturates due to non-linear evolution in standard gravity (although it is also not far from the resolution limit of the experiment). We speculate that a similar phenomena would occur in modified gravity and smaller scales are not expected to carry significant additional information. Note that it is the *source* structures in which information saturates. At smaller scales the lensing spectrum would continue to carry information [42] if it could be reconstructed. For the smaller telescope the scale is limited to $\ell < 425$ by the resolution at the high end of the redshift window. If the redshift window were subdivided into narrower bins, it would be possible to use information at scales down to $\ell \approx 1000$ in the centre bins as at these redshifts the telescope resolutions are better and structures are less non-linear. However, considering tomographic information is beyond the scope of this work. It is noted that these scales are very large by weak lensing standards where optical surveys typically make detections down to an ℓ of order 10^5 .

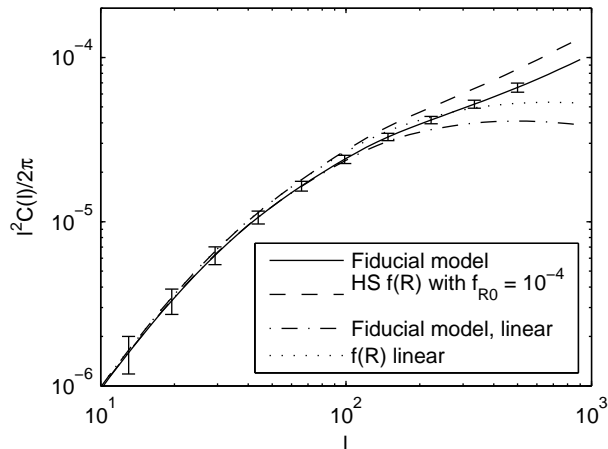


FIG. 1: The Weak lensing convergence power spectra for Λ CDM and the HS $f(R)$ model with $n = 1$ and $f_{R0} = 10^{-4}$. Galaxy distribution function is flat between $z = 1$ and $z = 2.5$.

C. External Priors from Planck

While the CMB is not sensitive to the late time effects of modified gravity (except by the integrated Sachs-Wolfe effect), it is invaluable for constraining other parameters and breaking degeneracies. As such, projected information from the Planck experiment is included. The Planck covariance matrix used here is given in [43, Table II]. All late time cosmological parameters (including the curvature) are marginalized over, removing information contained in the ISW effect, and ensuring that sensitivity to $f(R)$ is entirely from 21 cm tests below. The only remaining parameter that is related to the late time expansion is θ_s , the angular size of the sound horizon, which is then used as a constraint on the parameter sets of the modified gravity models.

IV. RESULTS

To quantify the projected constraints on $f(R)$ models, the Fisher matrix formalism is employed. The HS $f(R)$ models reduce to the fiducial model for vanishing f_{R0} and any value of n . Thus the Fisher Matrix formalism is used to project constraints on f_{R0} for given values of n . In the case of DGP, which does not reduce to the fiducial model, it is shown that a measurement consistent with the fiducial model can not be consistent with DGP for any parameter set. Unless otherwise noted, we account for freedom in the full cosmological parameter set: h , ω_m , ω_b , ω_k , A_s and n_s ; representing the Hubble parameter; physical matter, baryon and curvature densities; amplitude of primordial scalar fluctuations and the spectral index; respectively.

Within the $f(R)$ models, the fiducial model is a special point in the parameter space as there are no modifica-

tions to gravity. As such, one cannot in general expect perturbations to observables to be linear in the $f(R)$ parameter f_{R0} , an assumption implicit in the Fisher Matrix formalism. This assumption does seem to hold for the expansion history, where our first order perturbative calculation agrees with the full solution to the modified Friedmann Equations calculated in [18]. However, this is not the case for weak lensing. For each $f(R)$ model, the lensing spectrum was calculated for several values of f_{R0} . It was observed that enhancements to the lensing power spectrum go as

$$C^{\kappa\kappa}(\ell) - C_{fiducial}^{\kappa\kappa}(\ell) \sim (f_{R0})^{\alpha(\ell)}$$

with $\alpha(\ell)$ in the 0.5–0.7 range. This is because the reach of the enhanced forces in $f(R)$ is a power law in f_{R0} following Equation (3), and the enhancement of the power spectrum for a given mode k roughly scales with the time that this mode has been within the reach of the enhanced force. Because of this behaviour, the constraints derived within the Fisher Matrix formalism depend on the step size in f_{R0} used for finite differences.

To correct for this, we use a step size that is dependent on the final constraint. The weak lensing Fisher Matrices were calculated for f_{R0} step sizes of 10^{-3} , 10^{-4} and 10^{-5} . These were then interpolated—using a power law—such that the ultimate step size used for finite differences is roughly the quoted constraint on the modified gravity parameter. For instance when the 95% confidence constraint on f_{R0} is quoted, the step size for finite differences is $\Delta f_{R0} \approx 2\sigma_{f_{R0}}$, where $\sigma_{f_{R0}}$ is calculated from the interpolated Fisher matrix. This is expected to be valid down to step sizes at the 10^{-6} level where the chameleon mechanism is important. As such, for constraints below 10^{-5} a step size of 10^{-5} is always used. Note that this is conservative because an over sized finite difference step always *underestimates* the derivative of a power law with an power less than unity. For constraints above the 10^{-3} level a step size of 10^{-3} is used, which is the largest modification to gravity simulated. These constraints are considered unreliable due to these difficulties. We reiterate this this only affects results that include weak lensing information. Likelihood contours remain perfect ellipses in this procedure (which is clearly inaccurate), however the spacing between contours at different confidence levels is altered.

Figure 2 shows the projected constraints on the HS $f(R)$ model with $n = 1$ for various combinations of observational techniques, and a $(200\text{m})^2$ telescope. The elements in the lensing fisher matrix associated with the curvature are taken to be zero for the reasons given in Section III B. While this assumption is not conservative, it is expected to be valid, as the angular diameter distance as measured by the BAO is very sensitive to the curvature. In total three $f(R)$ models were considered: HS with $n = 1, 2, 4$. The results are summarized in Table I.

It was found that while weak lensing, in the linear regime, is very sensitive to the modifications to grav-

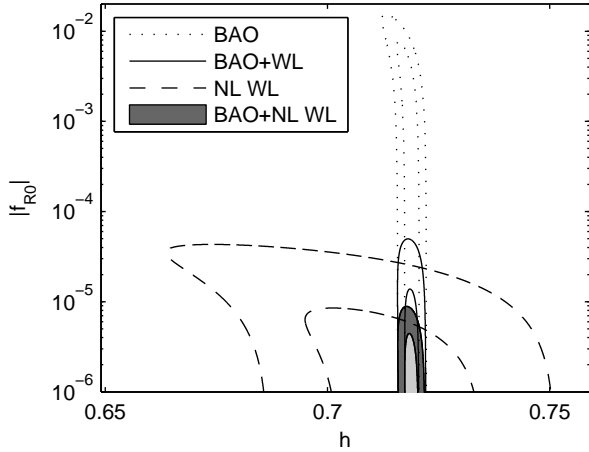


FIG. 2: Projected constraints on the HS $f(R)$ model with $n = 1$ using several combinations of observational techniques, for a 200 m telescope. All curves include forecasts for Planck. Allowed parameter values are shown in the $f_{R0} - h$ plane at the 68.3%, and 95.4% confidence level. Results are not shown for “WL” which were calculated much less accurately (see text).

95% confidence upper limits	HS $ f_{R0} $			
	$n = 1$	NL WL	$n = 2$	$n = 4$
BAO	1.5e-02	~	1.8e-02	3.0e-02
WL	2.3e-03	4.3e-05	4.0e-03	8.6e-03
BAO+WL	5.0e-05	8.9e-06	9.7e-05	4.6e-04

TABLE I: Projected constraints on $f(R)$ models for various combinations of observational techniques, for a 200 m telescope. Constraints are the 95% confidence level upper limits and include forecasts for Planck. The non linear results (column marked NL WL) are for the HS model with $n = 1$. Results that make use of weak lensing with constraints above 10^{-3} are only order of magnitude accurate. The linear regime is taken to be $\ell < 140$, with the nonlinear constraints extending up to $\ell = 600$.

ity, it is only barely capable of constraining $f(R)$ models without separate information about the expansion history. Even with the inclusion of Planck forecasts, degeneracies with h and ω_k , the mean curvature, drastically increase the uncertainties on the modified gravity parameters. Indeed these three parameters are more than 95% correlated (depending on the exact model and confidence interval). This of course brings into question the neglect of the ω_k terms in the weak lensing Fisher Matrix. However it is noted that in these cases, the predicted limits on the curvature are $|\omega_k| < 0.025$ at 95% confidence. The current, model independent, limits on the curvature using WMAP, SDSS and HST data are approximately half this value [44]. Our neglect of any direct probes of the expansion history for the Planck+WL constraints is clearly unrealistic; however, the constraints illustrate what is actually measured by weak lensing. In any case

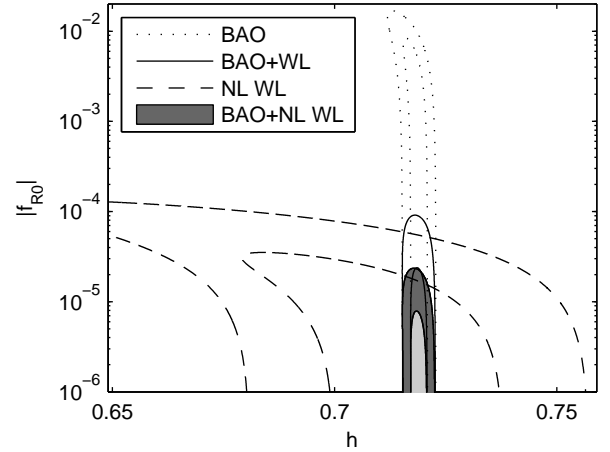


FIG. 3: Same as Figure 2 but for a 100 m cylindrical telescope.

these degeneracies are broken once BAO measurements are included, and in this final case the modified gravity parameters are correlated with the other parameters by at most 35%. Also, considering lensing in the nonlinear regime breaks the degeneracy to a certain extent.

First generation cylindrical telescopes will likely be smaller than the one considered above. To illustrate the differences in constraining ability, we now present a few results for a cylindrical radio telescope that is 100m on the side. Reducing the resolution of the experiment degrades measurements in a number of ways. BAO measurements become less than ideal in the higher redshift bins. The smallest scale that can be considered for weak lensing drops to about $\ell = 425$. A more important effect is that the lensing spectra can not be as accurately reconstructed, dropping the effective galaxy density down to $n_g/\sigma_e^2 = 0.22$. Figure 3 shows analogous results to 2 but for a telescope with half the resolution.

To show that a set of measurements consistent with the fiducial model would be inconsistent with DGP we first fit DGP to the fiducial model’s CMB and BAO expansion history by minimizing

$$\tilde{\chi}^2 = (\mathbf{r}_{DGP} - \mathbf{r}_{fiducial})^T C^{-1} (\mathbf{r}_{DGP} - \mathbf{r}_{fiducial}) \quad (16)$$

where \mathbf{r}_{DGP} and $\mathbf{r}_{fiducial}$ are vectors of observable quantities as calculated in the DGP and fiducial models, and C is the covariance matrix. \mathbf{r} includes BAO $d_A(z)$ and $H(z)$ as well as Planck priors on ω_m and θ_s . Note that $\tilde{\chi}^2$ is not truly chi-squared since $\mathbf{r}_{fiducial}$ contains fiducial model predictions and is not randomly distributed like a real data set.

Performing the fit yields DGP parameters: $h = 0.677$, $\omega_m = 0.112$, $\omega_k = -0.0086$ and $\omega_{rc} = 0.067$. Figure 4 shows the deviation of H and d_A respectively for the best fit DGP model compared to the fiducial model. $\tilde{\chi}^2 = 332.8$ for the fit despite there only being 16 degrees of freedom, and as such a measurement consistent with the fiducial model would thoroughly rule out DGP.

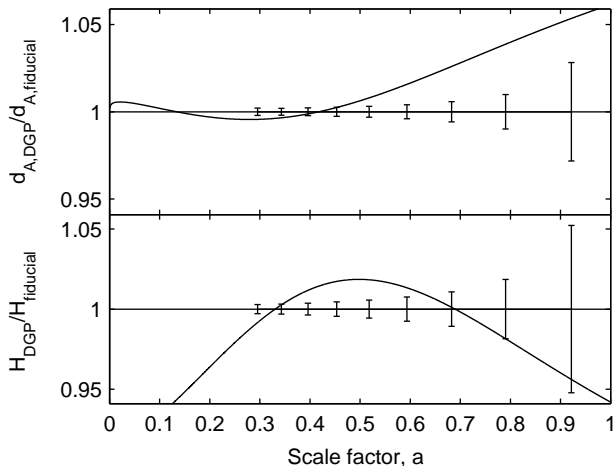


FIG. 4: Ratio of the coordinate $d_A(z)$ (top) and the Hubble parameter $H(z)$ (bottom) as predicted by the best fit DGP model to the fiducial model. Error bars are from 21 cm BAO predictions. Fit includes BAO data available from the 200 m telescope and CMB priors on θ_s and ω_m .

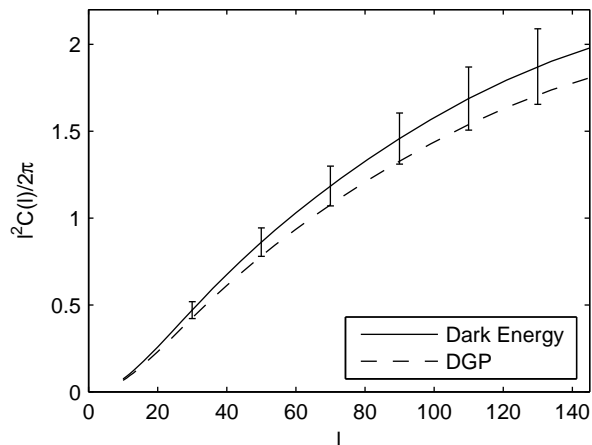


FIG. 5: Weak lensing spectra in for DGP and a smooth dark energy model with the same expansion history. DGP parameters are $h = 0.665$, $\omega_m = 0.116$, $\omega_k = 0$ and $\omega_{rc} = 0.06$. Errorbars represent expected accuracy of the 200 m telescope.

In the case that expansion history measurements are consistent with DGP, the question arises as to whether DGP could be distinguished from a smooth dark energy model that had the same expansion history. The additional information in linear perturbations as measured by weak lensing allows DGP to be distinguished even from a dark energy model with an identical expansion history. Figure 5 shows the lensing spectra for a DGP cosmology similar to the best fit discussed above, as well as the dark energy model with the same expansion history as in [29].

In principle one should consider the small amount of freedom within the DGP parameter set that could be

used to make the DGP spectrum better fit the dark energy spectra. However this is unlikely to significantly change the spectrum as all relevant parameters are tightly constrained by the CMB and BAO. For example it is clear from Figure 5 that the lensing spectra of the two models would better agree if the amplitude of primordial scalar perturbations was increased in the DGP model. However, Planck measurements would only allow of order half a percent increase while the disagreement is of order 10%. This is somewhat justified by the lack of correlations found in the $f(R)$ fisher matrices once all three observational techniques are included. In addition we have not considered information from weak lensing in the nonlinear regime. Adding nonlinear scales would only make our conclusion that DGP and smooth dark energy are distinguishable with these observations more robust.

V. DISCUSSION

We have shown that the first generation of 21 cm intensity mapping instruments will be capable of constraining the HS $f(R)$ model (with $n = 1$) down to a field value of $|f_{R0}| \lesssim 2 \times 10^{-5}$ at 95% confidence (Figure 3). This is an order of magnitude tighter than constraints currently available from galaxy cluster abundance [19]. Furthermore, model parameters in this regime are not ruled out by Solar System tests.

In comparing Figures 2 and 3 it is clear that a more advanced experiment, with resolution improved by a factor of two, would further half the allowed value of $|f_{R0}|$. It should be noted however, that halving of the allowed parameter space does not correspond to a factor of four increase in information. Deviations in the lensing spectrum scale sub-linearly in the $f(R)$ parameters, enhancing the narrowing of constraints as information is added (see Section IV).

While we have concentrated on a particular $f(R)$ model, many viable functional forms for $f(R)$ have been proposed in the literature [45–47]. The predictions for the growth of structure in these different models agree qualitatively: the gravitational force is enhanced by $4/3$ within λ_C , enhancing the growth on small scales. However, there are quantitative differences in the model predictions due to the different evolution of λ_C over cosmic time. Our results for the HS model with different values of n should thus cover a range of different functional forms for $f(R)$. Table I shows that our constraints do not depend very sensitively on the value of n . This is because the weak lensing measurements cover a wide range of scales as well as redshifts. Furthermore, it is straightforward to map the enhancement in the linear $P(k, z)$ at given k and z from the HS model considered here to any other given model, to obtain approximate constraints for that model.

Future cluster constraints will almost certainly improve on the current limits of $|f_{R0}| \lesssim \text{few } 10^{-4}$ [19].

However, for smaller field values, the main effect of $f(R)$ gravity shifts to lower mass halos, since the highest mass halos are chameleon-screened (see Fig. 2 in [22]). Hence, future cluster constraints will depend on the ability to accurately measure the halo abundance at masses around few $10^{14} M_\odot$ and less. Furthermore, the constraints from cluster abundances depend sensitively on the knowledge of the cluster mass scale, and are already systematics-dominated [19]. Weak lensing constraints have a completely independent set of observational systematics, and are in principle less sensitive to baryonic or astrophysical effects. Thus, the forecasted constraints on modified gravity presented here are quite complementary to constraints from cluster abundances.

The processes that produce the BAO feature in the matter power spectrum are understood from first principles. In addition the BAO length scale can be extracted even in the presence of large uncertainties in biases and mass calibrations. Likewise, weak lensing on large scales is well understood, with baryonic physics being much less important than on smaller scales [48]. In addition the dominant systematics present in optical weak lensing surveys are instrumental in nature and not intrinsic to the quantities being measured. While 21 cm intensity mapping is as yet untested, instrumental systematics will be very different from those that affect the optical.

In the case of this study, and more generally for cosmological models which substantially modify structure formation, the motivation for higher resolution comes not from improved BAO measurements but from better weak lensing reconstruction. Higher resolution not only makes weak lensing information available at higher multi-poles, but improves the accuracy at which lensing can be reconstructed on all scales.

The inclusion of lensing information in the nonlinear regime was crucial, and largely responsible for the competitiveness of these forecasts. As seen in Figure 1, much of the constraints come from multi-poles in the nonlinear regime. It should be noted that for the higher resolution experiment considered, the minimum scale is limited not by the resolution at high redshift, but by the saturation of information in nonlinear source structures at low redshift [36].

Our constraints from lensing are conservative since only one wide source redshift bin was considered, limited to $\ell < 600$ as described above. To maximize information, the source redshift range could be split into multiple bins, properly considering the correlation in the lensing signal between them; a process known as lensing tomography. The low redshift bin would be limited as above, and the high redshift bin would be limited by the resolution to $\ell \approx 850$ at $z = 2.5$. However in intermediate bins, the lensing signal could be reliably reconstructed above $\ell \approx 1000$.

Unlike most smooth dark energy models, such as quintessence, constraints on the models considered here are chiefly sensitive to structure formation, as is clear from Figure 2. No experiment in the foreseeable future will be able to improve upon the constraints we project on these models using exclusively expansion history probes (except by breaking degeneracies). These forecasts show that 21 cm intensity mapping is not only sensitive to a cosmology's expansion history through the BAO, but also to structure growth through weak lensing. The weak lensing measurements cannot compete with far off space based surveys like Euclid or JDEM, which will have galaxy densities of order 100 arcmin^{-2} [8] and resolution to far greater ℓ . However, cylindrical 21 cm experiments are realizable on a much shorter time scale and at a fraction of the cost. In addition, the measurements considered here are approaching the limit at which $f(R)$ models can be tested. For $|f_{R0}|$ much less than 10^{-6} the chameleon mechanism becomes important before there are observable modifications to structure growth, reducing the motivation to further study these models.

It has also been shown that, for these experiments, a BAO measurement consistent with Λ CDM would definitively rule out DGP without a cosmological constant as a cosmological model. Even in the case that a BAO measurement consistent with DGP is made, the model is still distinguishable from an exotic smooth dark energy model through structure growth. The former result is not surprising given that DGP is now in conflict with current data [29]. However it is illustrative that a single experiment can precisely probe both structure formation and expansion history. Even a dark energy model that conspires to mimic DGP is, to a large extent, distinguishable.

We have studied the effects of modified gravity theories on observational quantities for future 21 cm surveys. Because these surveys measure the distribution of galaxies on large angular scales over large parts of the sky, they are well suited to measure the expected deviations relative to standard general relativity. We have computed the predictions of modified gravity in the linear and nonlinear regimes, and compared to the sensitivity of future surveys. We find that a large part of parameter space can be tested.

Acknowledgments

We would like to thank Tingting Lu for helpful discussions. KM is supported by an NSERC Canadian Graduate Scholars-M scholarship. FS is supported by the Gordon and Betty Moore Foundation at Caltech. PM acknowledges support of the Beatrice D. Tremaine Fellowship.

[1] L. Knox, Y.-S. Song, and J. A. Tyson, Phys. Rev. D **74**, 023512 (2006).

[2] B. Jain and P. Zhang, ArXiv e-prints **709** (2007),

- 0709.2375.
- [3] S. Tsujikawa and T. Tatekawa, ArXiv e-prints **804** (2008), 0804.4343.
 - [4] F. Schmidt, Phys. Rev. **D78**, 043002 (2008), 0805.4812.
 - [5] J. B. Peterson et al. (2009), 0902.3091.
 - [6] H.-J. Seo et al. (2009), 0910.5007.
 - [7] T.-C. Chang, U.-L. Pen, J. B. Peterson, and P. McDonald, Phys. Rev. Lett. **100**, 091303 (2008), 0709.3672.
 - [8] A. J. Albrecht et al. (2006), astro-ph/0609591.
 - [9] S. M. Carroll, V. Duvvuri, M. Trodden, and M. S. Turner, Phys. Rev. D **70**, 043528 (2004), arXiv:astro-ph/0306438.
 - [10] A. A. Starobinsky, Phys. Lett. **B91**, 99 (1980).
 - [11] S. Capozziello, Int. J. Mod. Phys. **D11**, 483 (2002), gr-qc/0201033.
 - [12] T. P. Sotiriou and V. Faraoni (2008), 0805.1726.
 - [13] S. Nojiri and S. D. Odintsov, Phys. Rev. **D68**, 123512 (2003), hep-th/0307288.
 - [14] I. Sawicki and W. Hu, Phys. Rev. **D75**, 127502 (2007), astro-ph/0702278.
 - [15] S. Nojiri and S. D. Odintsov, Phys. Rev. **D74**, 086005 (2006), hep-th/0608008.
 - [16] Y.-S. Song, H. Peiris, and W. Hu, Phys. Rev. **D76**, 063517 (2007), 0706.2399.
 - [17] T. Chiba, Physics Letters B **575**, 1 (2003), ISSN 0370-2693.
 - [18] W. Hu and I. Sawicki, Phys. Rev. **D76**, 064004 (2007), 0705.1158.
 - [19] F. Schmidt, A. Vikhlinin, and W. Hu, Phys. Rev. D **80**, 083505 (2009), 0908.2457.
 - [20] H. Oyaizu, Phys. Rev. D **78**, 123523 (2008), 0807.2449.
 - [21] H. Oyaizu, M. Lima, and W. Hu, Phys. Rev. D **78**, 123524 (2008), 0807.2462.
 - [22] F. Schmidt, M. Lima, H. Oyaizu, and W. Hu, Phys. Rev. D **79**, 083518 (2009), 0812.0545.
 - [23] M. C. B. Abdalla, S. Nojiri, and S. D. Odintsov, Class. Quant. Grav. **22**, L35 (2005), hep-th/0409177.
 - [24] A. V. Frolov, Phys. Rev. Lett. **101**, 061103 (2008), 0803.2500.
 - [25] S. Nojiri and S. D. Odintsov, Phys. Rev. **D78**, 046006 (2008), 0804.3519.
 - [26] G. R. Dvali, G. Gabadadze, and M. Porrati, Phys. Lett. **B485**, 208 (2000), hep-th/0005016.
 - [27] C. Deffayet, Phys. Lett. **B502**, 199 (2001), hep-th/0010186.
 - [28] C. Deffayet, G. R. Dvali, and G. Gabadadze, Phys. Rev. **D65**, 044023 (2002), astro-ph/0105068.
 - [29] W. Fang et al., Phys. Rev. **D78**, 103509 (2008), 0808.2208.
 - [30] K. Koyama and R. Maartens, Journal of Cosmology and Astro-Particle Physics **1**, 16 (2006), arXiv:astro-ph/0511634.
 - [31] K. Koyama and F. P. Silva, Phys. Rev. D **75**, 084040 (2007), arXiv:hep-th/0702169.
 - [32] R. Scoccimarro, ArXiv e-prints (2009), 0906.4545.
 - [33] A. Lue, R. Scoccimarro, and G. D. Starkman, Phys. Rev. D **69**, 124015 (2004), arXiv:astro-ph/0401515.
 - [34] F. Schmidt, Phys. Rev. D **80**, 043001 (2009), 0905.0858.
 - [35] H.-J. Seo and D. J. Eisenstein, Astrophys. J. **665**, 14 (2007), arXiv:astro-ph/0701079.
 - [36] T. Lu, U.-L. Pen, and O. Dore (2009), 0905.0499.
 - [37] A. Lewis, A. Challinor, and A. Lasenby, Astrophys. J. **538**, 473 (2000), astro-ph/9911177.
 - [38] A. Lewis and A. Challinor, Phys. Rev. **D76**, 083005 (2007), astro-ph/0702600.
 - [39] R. E. Smith, J. A. Peacock, A. Jenkins, S. D. M. White, C. S. Frenk, F. R. Pearce, P. A. Thomas, G. Efstathiou, and H. M. P. Couchman, MNRAS **341**, 1311 (2003), arXiv:astro-ph/0207664.
 - [40] W. Hu and I. Sawicki, Phys. Rev. D **76**, 104043 (2007), arXiv:0708.1190.
 - [41] D. J. Eisenstein and W. Hu, Astrophys. J. **496**, 605 (1998), arXiv:astro-ph/9709112.
 - [42] O. Dore, T. Lu, and U.-L. Pen (2009), 0905.0501.
 - [43] P. McDonald and D. Eisenstein, Phys. Rev. **D76**, 063009 (2007), astro-ph/0607122.
 - [44] E. Komatsu et al. (2010), 1001.4538.
 - [45] S. Nojiri and S. D. Odintsov, Phys. Lett. **B657**, 238 (2007), 0707.1941.
 - [46] A. A. Starobinsky, JETP Lett. **86**, 157 (2007), 0706.2041.
 - [47] S. A. Appleby and R. A. Battye, Phys. Lett. **B654**, 7 (2007), 0705.3199.
 - [48] H. Zhan and L. Knox, Astrophys. J. **616**, L75 (2004), astro-ph/0409198.